Fall run 2018 – analysis report

W. Schreyer

March 13, 2019

Contents

1 Introduction

This document describes several analyses of the data taken during the 2018 run of the UCN source at TRIUMF, covering measurements of

- transmission through guide components
- storage lifetime in the source, and
- storage lifetime in guide components.

All these experiments are performed in cycles. Each cycle contains several periods, typically starting with an irradiation period, during which the target is irradiated with protons and ultracold neutrons are produced. This can be followed by up to 9 more periods, like storage or detection periods. For each period, up to 8 UCN components like valves or spin flippers can be to set

different states. The last (11th) period covers the time until the next irradiation and cycle starts.

Cycles with different period durations and valve settings can be grouped in supercycles, which can be repeated several times. Cycles of one experiment can be spread over several Midas runs.

Two UCN detectors were used throughout the run. A Li6 detector, detecting scintillation light of UCN captured in ^{6}Li-enriched glass, and a He3 detector, detecting gas discharges due to UCN captured by ^{3}He. Experiments can use either detector alone or both at the same time.

2 Preparation of raw detector data

The Li6 detector uses two values to determine if a detected event was actually caused by a UCN: "PSD" based on the pulse shape of the event and Q_{long}, the charge collected during a 200 ns window after the event trigger. An event is considered a UCN if

$$\text{PSD} > 0.3 \tag{1}$$

and

$$Q_{\text{long}} > 2000. \tag{2}$$

The He3 detector considers an event to be a UCN if the charge collected after the event trigger

$$Q_{\text{short}} > 300. \tag{3}$$

3 Transmission measurements

Transmission measurements are experiments with two periods per cycle. An irradiation period, where UCN are produced and a small percentage is detected in the He3 detector connected to a monitoring port, while a valve downstream of the He3 detector is closed. And a counting period, where the UCN valve is opened and UCN transmitted through components downstream of the valve are detected in the Li6 detector.

The number of UCN detected in the He3 "monitor" detector during irradiation is a direct measure of the number of UCN actually produced by the source. The ratio of the number of UCN detected in the Li6 detector during the detection period to the "monitor counts" therefore is directly proportional to how many of the produced UCN could be transmitted through the guide components downstream of the valve. To compare the transmission through guide components in two different setups, we can divide the ratios from each of those setups.

A constant background rate b^{Li6} (see section 6) is subtracted from the number of UCN counted in the Li6 detector during counting $C^{\text{Li6}}_{\text{counting}}$:

$$N^{\text{Li6}}_{\text{counting}} = C^{\text{Li6}}_{\text{counting}} - b^{\text{Li6}} \cdot t_{\text{counting}}, \tag{4}$$

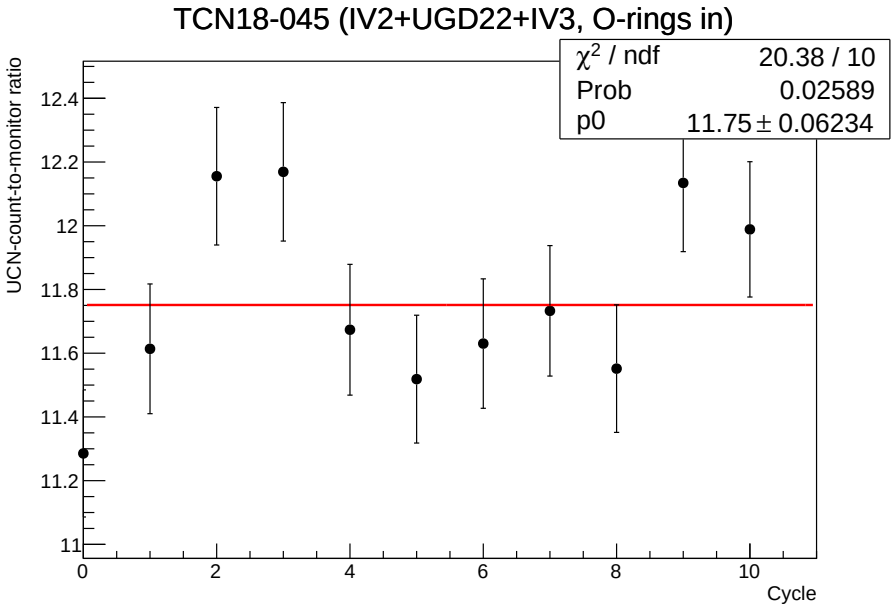

Figure 1: Ratio of Li6 counts to He3 counts for all cycles of transmission experiment TCN18-045, fitted with a constant function. The legend shows the χ^2/ν of the fit, the average ratio $\bar{R}$, and its uncertainty.

with an uncertainty

$$\Delta N^{\mathrm{Li6}}_{\mathrm{counting}} = \sqrt{\sqrt{C^{\mathrm{Li6}}_{\mathrm{counting}}}^{2} + \left(\Delta b^{\mathrm{Li6}} \cdot t_{\mathrm{counting}}\right)^2}. \tag{5}$$

Then the background-corrected count $N^{\mathrm{Li6}}_{\mathrm{counting}}$ is divided by the number of UCN detected in the He3 detector during the irradiation period $N^{\mathrm{He3}}_{\mathrm{irradiation}}$

$$R = \frac{N^{\mathrm{Li6}}_{\mathrm{counting}}}{N^{\mathrm{He3}}_{\mathrm{irradiation}}}, \tag{6}$$

with an uncertainty

$$\Delta R = \sqrt{\left(\frac{\Delta N^{\mathrm{Li6}}_{\mathrm{counting}}}{N^{\mathrm{He3}}_{\mathrm{irradiation}}}\right)^2 + \left(\sqrt{N^{\mathrm{He3}}_{\mathrm{irradiation}}}\,\frac{N^{\mathrm{Li6}}_{\mathrm{counting}}}{{N^{\mathrm{He3}}_{\mathrm{irradiation}}}^{2}}\right)^2}, \tag{7}$$

The He3 detector is assumed to be background-free[1].

The ratios for all cycles are plotted using ROOT. A χ^2 fit of a constant function over all cycles is used to determine the average $\bar{R}$ and its uncertainty $\Delta\bar{R}$, see figure 1.

[1]The expected number of background counts is about 6, while the total count during irradiation varies between 2000 and 4000

The relative transmission T of one experiment compared to another is

$$T = \frac{\bar{R}_1}{\bar{R}_2} \tag{8}$$

with the uncertainties for each $\bar{R}$ scaled by the χ^2 per degrees of freedom ν from the fit:

$$\Delta T = T\sqrt{\left(\frac{\Delta\bar{R}_1\chi_1^2}{\bar{R}_1\nu_1}\right)^2 + \left(\frac{\Delta\bar{R}_2\chi_2^2}{\bar{R}_2\nu_2}\right)^2}. \tag{9}$$

3.1 Time of flight

The transmission experiments also allow us to study how transmission changes over time. Following the same scheme shown above, we look at the background-corrected number of counts detected in the Li6 detector in narrow time bins $\Delta t = t_{i+1} - t_i$ after the valve opened

$$N_{t_i}^{\mathrm{Li6}} = C_{t_i}^{\mathrm{Li6}} - b^{\mathrm{Li6}} \cdot \Delta t, \tag{10}$$

and normalize them to the number of UCN detected in the He3 detector during irradiation

$$R_{t_i} = \frac{N_{t_i}^{\mathrm{Li6}}}{N_{\mathrm{irradiation}}^{\mathrm{He3}}}. \tag{11}$$

The resulting time-binned histogram is averaged over all cycles using ROOT, see figure 2.

Dividing the histograms from two different transmission experiments shows how the relative transmission changes over time, see figure 3.

3.2 Excluded cycles

Individual cycles can be excluded from the analyzed transmission data if

- the beam current dropped below 0.1 µA (10 cycles);
- the beam current fluctuated by more than 0.02 µA (10 cycles);
- the last period does not contain any Li6 events, i.e. the run was aborted at some point during this cycle (34 cycles);
- the He3 detector detected less than 1000 UCN during irradiation (6 cycles);
- the ion gauge IG6 read a pressure between 10^{-7} torr and 10^{-2} torr, indicating that it was on, causing additional background in the Li6 detector (62 cycles);
- the Li6 detector detected an average rate below 10 Hz during the counting period (0 cycles); or

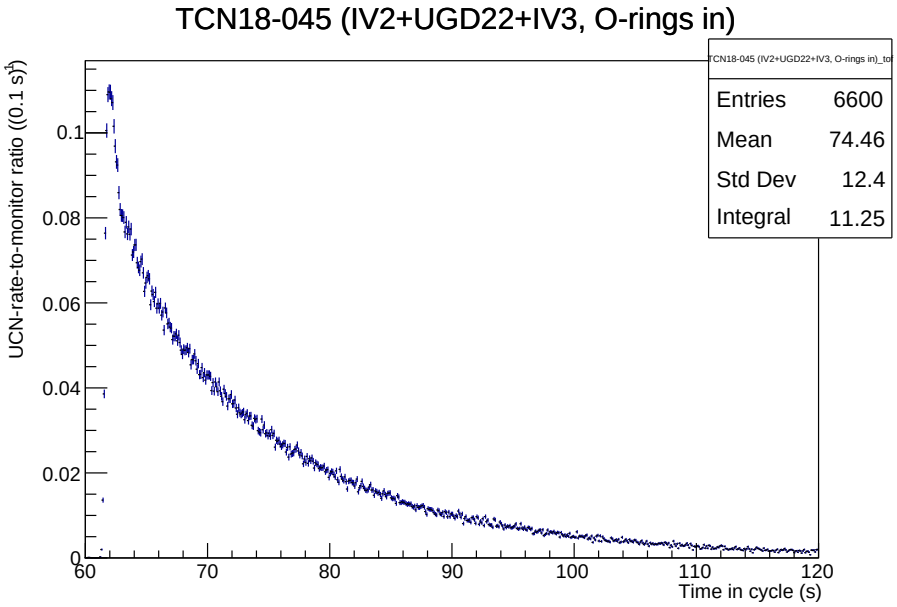

Figure 2: Rate in the Li6 detector after opening the valve during transmission experiment TCN18-045, normalized to the He3 detector and averaged over all cycles.

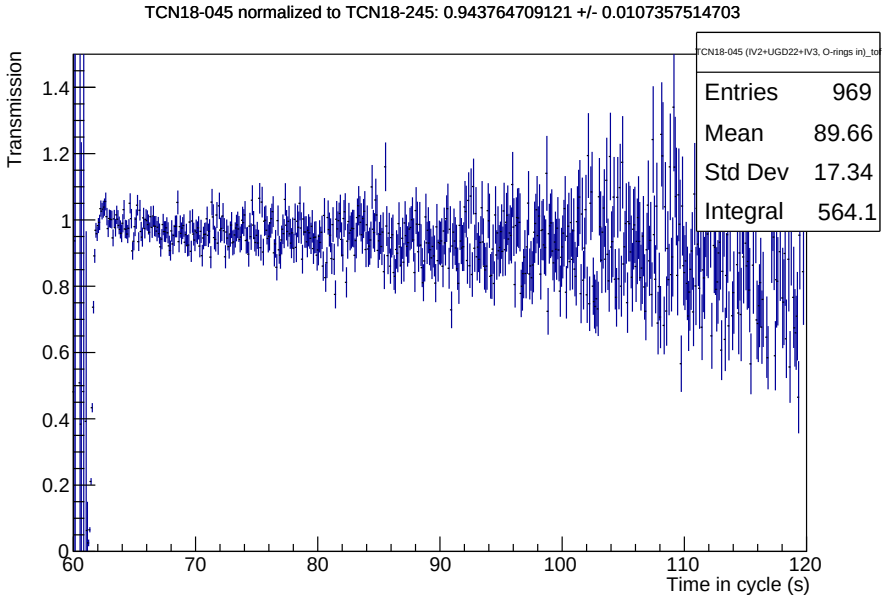

Figure 3: Ratio of normalized rates in experiment TCN18-045 and TCN18-245. The title contains the total relative transmission T.

- the Li6 detector detected a large background rate above 10 Hz during the irradiation period (4 cycles).

In total, 126 out of 541 cycles were excluded. All cycles of experiments TCN18-029 (run 934) and TCN18-080 (run 973) had to be discarded, due to IG6 being on.

3.3 Results

Table 1 lists the results of the individual transmission experiments and table 2 compares several.

The most striking result is that the identical reference experiments TCN18-045 and TCN18-245 performed at different times do not agree. This suggests that some time between runs 954 and 1129 either the transmission, the detector efficiencies, the geometry upstream of IV2, or the UCN spectrum changed. Unfortunately another test of repeatability, TCN18-080, which was set up identically to TCN18-480, had to be discarded.

For now, the earlier transmission experiments up to run 1081 are compared to TCN18-045 and the later ones from run 1131 are compared to TCN18-245.

The ratio of time-of-flight histograms (Fig. 3) shows that transmission in the first few seconds of TCN18-045 is lower than in TCN18-245, suggesting that there also is some timing discrepancy.

Table 1: Results of transmission experiments. If not otherwise noted, all transmission measurements were performed with the listed guides between IV2 and IV3, the IVs' O-rings pointing towards each other, and a 90° elbow downstream of IV3. The χ^2 gives an indication of how well the data fits the assumption that the ratio R stays constant over all cycles in each experiment.

Experiment	Run	$\bar{R}$	χ^2/ν	Description
TCN18-031	938	12.92 ± 0.06	1.90	IV2 + UGD17 + elbow
TCN18-035	944	11.81 ± 0.06	1.23	UGD22, O-rings of IVs pointing away from each other
TCN18-045	954	11.75 ± 0.06	2.04	UGD22
TCN18-053	985	11.27 ± 0.06	1.64	burst disk + UGD2
TCN18-085	973	11.29 ± 0.06	1.66	UGD22 + 19 (NiP)
TCN18-090	1000	10.96 ± 0.06	1.48	UGD22 + UGA11 + UGG3 + UGA5
TCN18-290	1009	11.08 ± 0.07	1.56	UGD22 + UGA5 + UGG3 + UGA6
TCN18-060	1013	11.38 ± 0.06	1.19	UGD10 + 17 + 11
TCN18-065	1054	11.20 ± 0.06	1.19	SCM warm bore
TCN18-265	1081	6.51 ± 0.04	0.62	SCM warm bore with foil
TCN18-115	1125	6.95 ± 0.04	2.57	UGD22 + 2 + Ti foil
TCN18-245	1129	12.45 ± 0.07	0.65	UGD22 (repeat)
TCN18-480	1131	12.12 ± 0.07	0.80	UGD22 + 2
TCN18-057	1141	11.73 ± 0.06	1.42	vent spider + UGD2
Experiments at high position:				
TCN18-302	1165	16.07 ± 0.07	1.89	IV2 + elbow + UGD10 + 18
TCN18-240	1176	9.95 ± 0.05	1.79	IV2 + elbow + UGD10 + Al foil + UGD18
TCN18-215	1181	7.14 ± 0.04	1.57	UGD22 + 20 + Ti foil
TCN18-380	1188	15.8 ± 0.08	3.07	UGD22 + 20
TCN18-310	1192	17.12 ± 0.07	1.56	UGD22 + 20, smooth elbow

Table 2: Comparison of transmission experiments.

Experiment	Reference	T	Description
TCN18-045	TCN18-245	0.944 ± 0.010	Comparison of reference measurements
TCN18-035	TCN18-031	0.912 ± 0.010	UGD22+IV3 compared to UGD17
TCN18-045	TCN18-035	0.994 ± 0.013	Flipping IV2 and IV3
TCN18-053	TCN18-045	0.959 ± 0.013	Replacing UGD22 with burst disk and UGD2
TCN18-085	TCN18-045	0.960 ± 0.014	Adding UGD19 (NiP)
TCN18-090	TCN18-045	0.932 ± 0.013	Adding UGG3 with UGA11+3
TCN18-290	TCN18-045	0.943 ± 0.013	Adding UGG3 with UGA5+6
TCN18-060	TCN18-045	0.969 ± 0.012	Replacing UGD22 with UGD10 + 17 + 11
TCN18-065	TCN18-045	0.953 ± 0.012	Replacing UGD22 with SCM warm bore
TCN18-265	TCN18-065	0.581 ± 0.004	Adding foil to SCM warm bore
TCN18-115	TCN18-480	0.573 ± 0.009	Adding Ti foil
TCN18-480	TCN18-245	0.974 ± 0.006	Adding UGD2
TCN18-057	TCN18-245	0.942 ± 0.008	Replacing UGD22 with vent spider and UGD2
Experiments at high position:			
TCN18-240	TCN18-302	0.619 ± 0.007	Adding Al foil
TCN18-215	TCN18-380	0.451 ± 0.008	Adding Ti foil
TCN18-310	TCN18-380	1.082 ± 0.019	Replacing kinked with smooth elbow

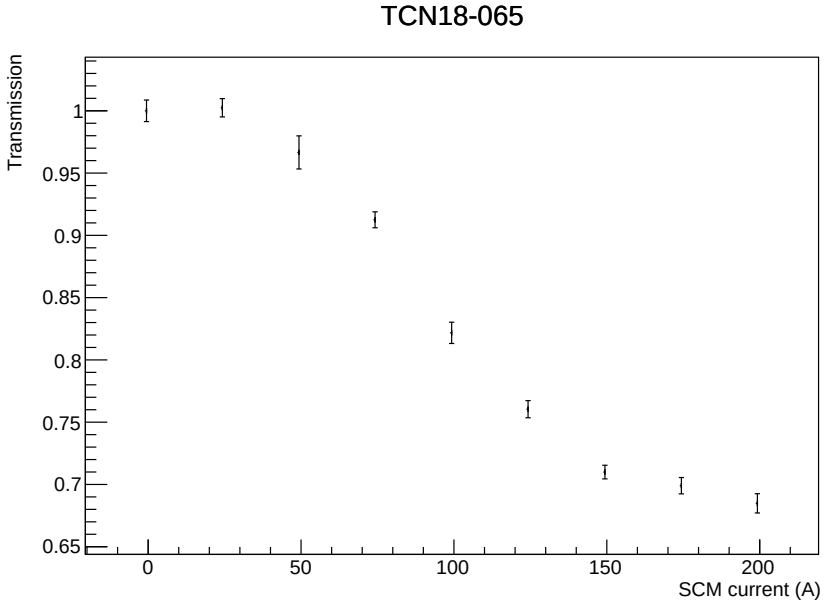

Figure 4: Transmission T through the warm bore while the SCM is powered with different currents, compared to transmission while unpowered.

3.4 SCM transmission

We equipped the superconducting polarizer magnet (SCM) with a "warm" bore with an inner diameter of 85 mm and an 0.1 mm thick AlMg3 foil in the center. Due to the tight fit of the guide through the cold superconducting magnet coil the foil could only be clamped between two narrow surfaces and was stripped out when we accidentally produced a pressure difference across the foil while pumping the guide. Hence, we did the first transmission measurements without a foil. We were able to insert a new foil soldered onto a thin stainless-steel ring later on and performed the same measurements with the foil inserted.

As seen in table 2, adding the warm bore without the foil reduced transmission to the Li6 detector by 5 %, and only by 2 % compared to stainless-steel guides with the same total length (TCN18-060), despite the gaps in the Wilson-style flanges holding the bore.

When the current in the SCM magnet is increased the magnetic field B acts as a potential wall or trough with $V = \pm 60.3\,\mathrm{neV\,T^{-1}} \cdot B$, depending on the UCN's spin polarization. UCNs with the wrong polarization (low-field seekers) cannot penetrate the potential if their energy is too low, so at higher currents a larger part of their spectrum is not transmitted and the total transmission drops.

At the maximum current of 200 A the central field was measured as 3.79 T, sufficient to polarize UCNs with energies up to 229 neV. Due to the geometry

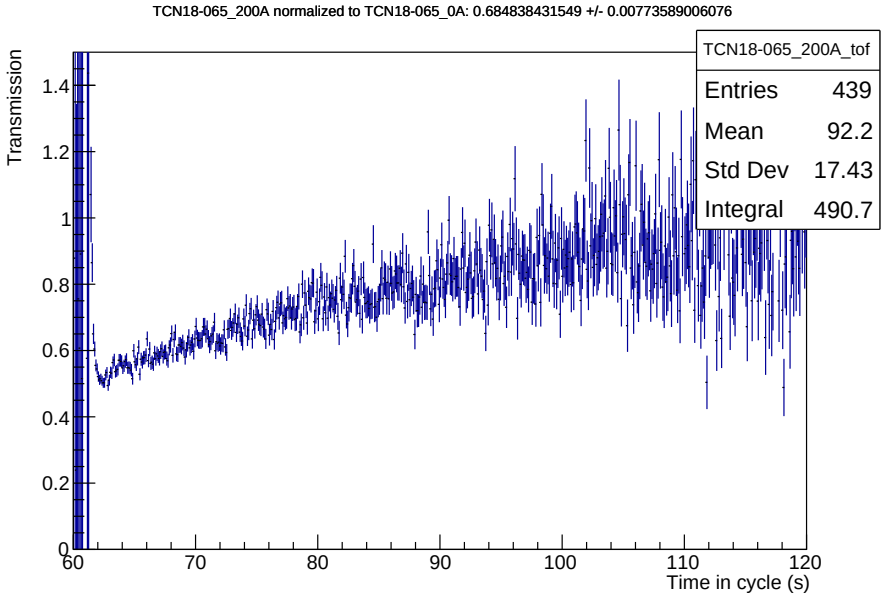

Figure 5: Normalized rate in the Li6 detector with the SCM at full current divided by the rate with no current.

of the source and UCN guides, we expect an energy range for UCNs roughly between 90 neV and 180 neV. This is confirmed by the transmission curve (Fig. 4) starting to drop at about 50 A, corresponding to $V = 70$ neV and leveling out at 150 A, corresponding to $V = 170$ neV. However, it does not drop to a transmission of 50 %, as we would expect if all low-field seekers are stopped by the magnetic field.

When comparing the UCN rates over time (Fig. 5), we see that the initial transmission at full current indeed drops to 50 % of the transmission at no current, and then slowly increases. This suggests that the low-field seekers trapped upstream of the SCM slowly depolarize and leak through the SCM.

When we inserted the foil, the transmission through the SCM with no current dropped by 42 % (Table 2). This drop is slightly higher than what we measured when adding the foil in experiment TCN18-240, most likely due to the stainless-steel ring and solder.

With the foil, the transmission curve starts to drop and level out at lower currents, since the aluminium foil adds its Fermi potential of 54 neV to the potential barrier. It also levels off at a higher relative transmission of 78 % and the initial time-resolved transmission at full current is much higher at 70 % (Fig. 7), since the magnetic field accelerates the high-field seekers and reduces their absorption in the foil, counteracting the loss of low-field seekers.

These effects have to be confirmed in simulation.

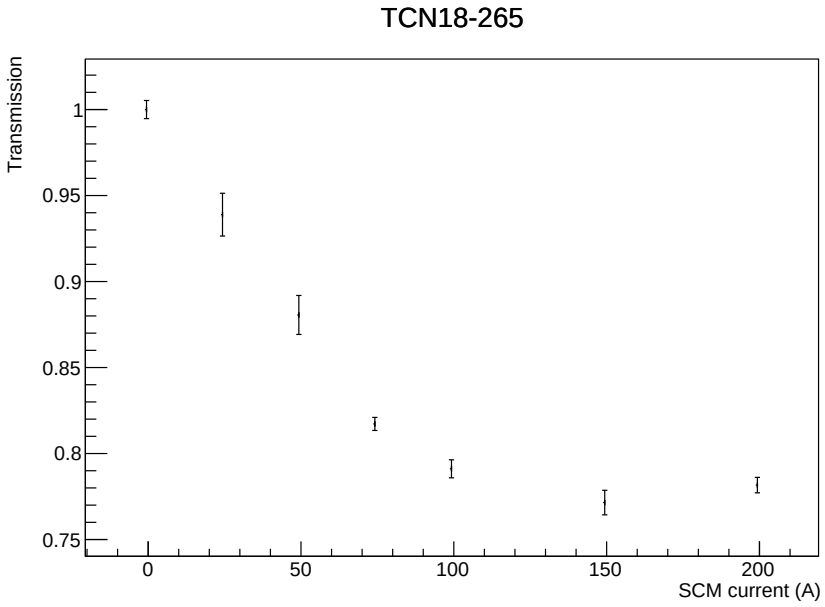

Figure 6: Transmission T through the warm bore with foil while the SCM is powered with different currents, compared to transmission while unpowered.

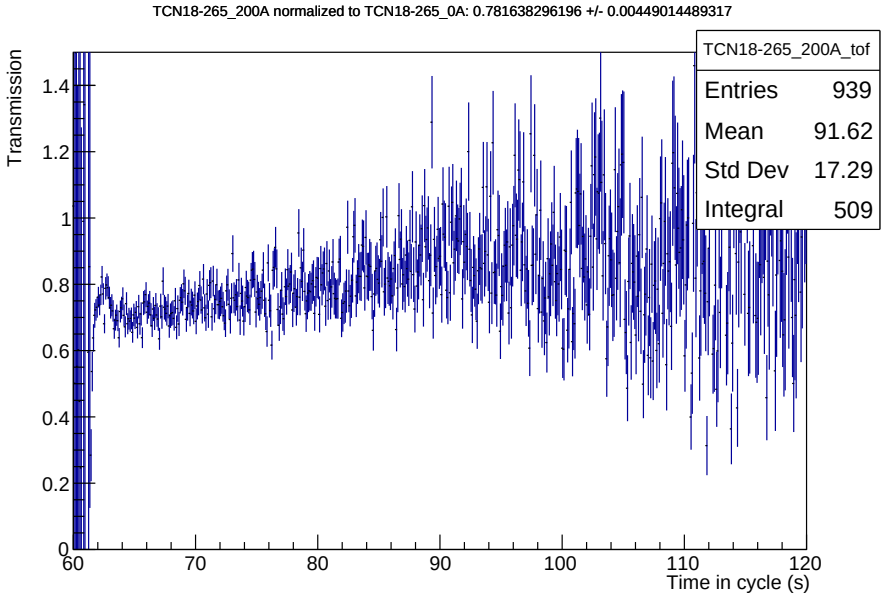

Figure 7: Normalized rate in the Li6 detector with the SCM at full current divided by the rate with no current, with the foil inserted.